Journal of Research and Applications in Mechanical Engineering
ISSN: 2229-2152 (Print); 2697-424x (Online)
(2021) Vol. 9, No. 1, Paper No. JRAME-21-9-009
[DOI: 10.14456/jrame.2021.9]

Research Article

TWO-DIMENSIONAL AXISYMMETRIC NUMERICAL STUDY OF THE PREMIXED COMBUSTION INSIDE THE POROUS MEDIA BURNER

K. Vithean[1]
J. Charoensuk[1]
K. Hanamura[2]
T. Sesuk[3]
V. Lilavivant[3,*]
[1] *School of Engineering, King Mongkut's Institute of Technology Ladkrabang, Bangkok 10520, Thailand*
[2] *Department of Mechanical Engineering, Tokyo Institute of Technology, Meguro-ku, Tokyo, 152-8552, Japan*
[3] *National Energy Technology Center (ENTEC), Pathum Thani 12120, Thailand*

Received 20 December 2020
Revised 11 February 2021
Accepted 9 March 2021

ABSTRACT:
Porous media combustion is one of the most efficient and has a wide-ranging application. Despite this, more investigation needs to be done in order to improve its efficiency and pollutant emission. In this research, the commercial simulation software is used to model and couple together the significant phenomena such as combustion, heat transfer, and fluid flow in porous media, which occur in this type of system. The free and porous media flow module was used to estimate fluid flow inside both fluid and porous media. Species formation and heat release during combustion were modeled by the transport of concentrated species module. Local thermal equilibrium was assumed for the energy equation and calculated by heat transfer in porous media module. Each physic was coupled together by two mechanisms—first, reaction flow, which coupled together between free and porous media flow and transport of concentrated species. Finally, nonisothermal flow coupled free and porous media flow with heat transfer in porous media. The combustion chamber, which is entirely filled with aluminum oxide pellets, is created for two dimensional axisymmetric. Physics-controlled mesh with finer element size is applied to generate mesh by the software to meet the specified need for each physic. Combustion behavior, velocity and temperature profile, and species formation are achieved from this simulation study.

Keywords: *CFD, Porous media combustion, Multiphysics simulation*

1. INTRODUCTION

The combustion of a hydrocarbon in porous media adds to the conventional burner, which produces high pollutant emission and low combustion efficiency, generate temperature higher than the adiabatic flame temperature. This is because the incoming fuel/air mixture gain some energy by heat recirculation from the reaction zone [1]. This type of combustion is commonly called excess enthalpy or super adiabatic combustion. Weinberg is one of the first researchers who introduced excess enthalpy burners through theoretical analysis [2]. Besides, this system not only generates high-temperature heat but also produces hydrogen via partial oxidation of methane for fuel cell applications [3].

Heat, which is the by-product of partial oxidation, can supply steam reforming energy which currently plays the dominant source for industrial hydrogen generation. Despite its advantages, the development of flame characteristics in porous media is essential in the research area. The topic can be well predicted by using the simulation tools.

* Corresponding author: V. Lilavivant
E-mail address: visarn.lil@entec.or.th

The study of porous media in three-dimensional space is essential because the flow behavior, temperature profile, species generation, and combustion characteristic can be detailed predicted. This method is required high computational power due to the complexity of the porous media geometry structure. Consequently, the study is feasible and time-saving by using the volume average method. Zhang et al. have made a comparison between the volume-average simulation and pore-scale simulation and compare both with the experimental data [4]. They conclude that the volume-averaged model is the precise and time-saving method compare with the pore-scale model. Therefore, two-dimensional asymmetry is utilized instead of three-dimensional, and a full chemical reaction mechanism such as GRI Mechanism 3.0 is replaced by the reduced mechanism.

Numerical analysis has been broadly used to research on porous media combustion. Sobhani et al. have investigated the pollutant emission and flame stability in porous media at a lean combustion regime [5]. The porous media burner was divided into two-layer and examined both numerically and experimentally. They conclude that the maximum stability limit occurred for the burner with Silicon Carbide at downstream and Yttria-stabilized Zirconia Alumina at upstream. The result also shows that the high level of CO formation occurs near flash-back conditions. The flame stability limit for lean methane-air porous media combustion is studied experimentally and numerically by Shi et al [6]. This research focuses on the profile of the flame stabilization and pollutant by modifying the equivalent ratio. They reported that the concentration of CO decreased by increasing the equivalent ratio while the flame stability limit increase as the equivalent ratio increase.

The main object of this study was to examine the flame behavior and pollutant emission in a porous media burner. The numerical simulations are performed by the commercial software COMSOL Multiphysics. There are three essential equations utilized for this simulation setup. Free and porous media flow was used to estimate fluid flow inside the system. Species evolution and heat release during combustion were modeled by the transport of concentrated species equation. Heat transfer between fluid and solid was calculated by using the heat transfer in porous media. Each physic was coupled together by two mechanisms—first, reaction flow, which coupled together between flow equation and transport of concentrated species. Second, nonisothermal flow, which coupled turbulent flow together with heat transfer. The combustion chamber, which is filled with porous media inside, is created two-dimensional axisymmetric. The physics-controlled mesh is performed to generate mesh by the software for each physic.

2. NUMERICAL MODEL

In this simulation, the computational domain is divided into two-part fluid domains (1, 3) and fluid and porous media domain (2), as illustrated in Fig. 1. The combustion zone is located with the fluid and porous media domain with a 0.05 m radius and 0.12 m length. The combustion chamber is filled with aluminum oxide pellets, whose diameter and porosity are 7.5 mm and 0.46, respectively. The heat capacity is 1000 J/(kg·K), the thermal conductivity is 25 W/(m·K), and the solid density of aluminum oxide is 3970 kg/m^3 [7]. Fuel and oxidizer enter at domain 1 which has a radius of 0.005 m. The outlet domain is 0.03 m in height and 0.05 m in radius. The domain is discretized by using a physics-controlled mesh which provides by the software. Extremely fine is chosen for the element size and contributed to all the modules. The total number degree of freedom is 265513 plus 7466 internal which is solved in this investigation.

2.1 Conservation equation

Conservation of mass

$$\nabla \cdot \left(\varepsilon_p \rho \boldsymbol{u} \right) = 0 \tag{1}$$

The momentum equation

$$\left(\rho \boldsymbol{u} \cdot \nabla \right) \boldsymbol{u} = -\nabla P + \nabla \cdot \mu \left(\left(\nabla \boldsymbol{u} + \left(\nabla \boldsymbol{u} \right)^T \right) - \frac{2}{3} \left(\nabla \cdot \boldsymbol{u} \right) \boldsymbol{I} \right) - \left(\nabla P \right)_p \tag{2}$$

For non-Darcian flow can be formulated as follow

$$-(\nabla P)_p = \left(\frac{\mu}{k} + \beta\rho|\boldsymbol{u}|\right)\boldsymbol{u} \tag{3}$$

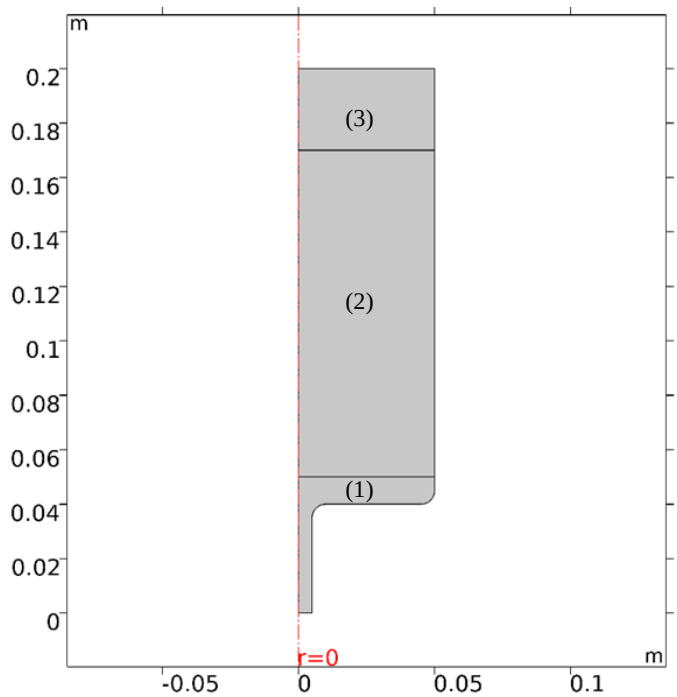

Fig. 1. Computational domain, fluid domain (1) and (3), and porous media domain (2).

The non-linear term in this equation is described by the Forchheimer equation

$$\beta = \frac{c_F}{\sqrt{k}} \quad \text{and} \quad k = \frac{d_p^2}{180} \times \frac{\varepsilon_p^3}{(1-\varepsilon_p)} \tag{4}$$

The local thermal equilibrium in porous media

$$\rho C_p \boldsymbol{u} \cdot \nabla T + \nabla \cdot (k_{eff} \nabla T) = Q + Q_{vd} \tag{5}$$

where

$$Q_{vd} = \tau : \nabla \boldsymbol{u} \tag{6}$$

Mass balance of each species

$$\nabla \cdot \mathbf{j}_i + \rho(\boldsymbol{u} \cdot \nabla) Y_i = q_i \tag{7}$$

where the mass flux can express as

$$\mathbf{j}_i = -\left(\rho D_i^m \nabla \mathrm{Y_i} + \rho \omega_i D_i^m \frac{\nabla M_n}{M_n} - \rho Y_i \sum\nolimits_k \frac{M_i}{M_n} D_k^m \nabla X_k + D_i^T \frac{\nabla T}{T}\right). \tag{8}$$

where

$$D_i^m = \frac{1 - Y_i}{\sum_{k \neq i} \frac{X_k}{D_{ik}}} \text{ and } M_n = \left(\sum_i \frac{Y_i}{M_i} \right)^{-1} \tag{9}$$

Ideal gas equation of state

$$\rho = \frac{PM_n}{Ru \cdot T} \tag{10}$$

2.1.1 Simplified reaction mechanism

It has been advised that the reduced reaction mechanism used in combustion modeling should represent the experimental flame properties or the detailed reaction mechanism for a wide range of initial temperatures, equivalence ratios, and pressure [8]. The single-step reaction has been applied to deal with lots of combustion problems because a few parameters are required to solve. However, this mechanism is not accurate for predicting temperature and species deformation. In this analysis, the two-step global reduced chemical reaction mechanism shortly called BFER's mechanism is adopted to describe the methane-air reaction which has been constructed using the methodology described [9]. BFER's mechanism has performed the test under a different range of inlet temperatures (300, 500, 700 K). pressure (1, 3, 10 atm) and ten equivalence ratios have been evaluated, ranging from 0.6 to 1.5, and then compare the result with GRI 3.0 full mechanism [10]. The result demonstrates that BFER's mechanism can execute well for the equivalence ratio of less than 1.4. Furthermore, it is the well-known reduced methane oxidation mechanism in large eddy simulation due to its simple and reliable reaction. Therefore, it is the most suitable candidate for this particular application.

The study of the chemical reaction is done in two steps. First, the reaction engineering module is applied to determine thermodynamic and transport data to the porous media combustion. The reduced chemical reaction is set for this case and Batch, the constant volume is selected as the reactor model. The second step is the multiphysics coupling of the chemistry module with the transport of concentrated species, heat transfer in porous media, and free and porous media flow module.

The simplified model uses five species namely methane (CH_4), oxygen (O_2), water (H_2O), carbon monoxide (CO), and carbon dioxide (CO_2) for two global reactions.

$$CH_4 + 1.5O_2 \rightarrow CO + 2H_2O \tag{11}$$

$$CO + 0.5O_2 \leftrightarrow CO_2 \tag{12}$$

The flame speed of the combustion was controlled by the first reaction. The second reaction is a reversible process that is included to estimate flame temperature accurately in the rich mixture condition.

For the compact notation of all mechanism

$$\sum_{i=1}^{N} v_{ij}^{'} X_i \leftrightarrow \sum_{i=1}^{N} v_{ij}^{''} X_i \quad \text{for} \quad j = 1, 2, \ldots, L \tag{13}$$

The net production rate of each species

$$\dot{\omega}_i = \sum_{j=1}^{L} v_{ij} q_j \quad \text{for} \quad i = 1, 2, \ldots, N \tag{14}$$

where

$$v_{ij} = \left(v_{ij}^{"} - v_{ij}^{'}\right) \text{ and } q_j = k_{fj}\prod_{i=1}^{N}\left[X_i\right]^{v_{ij}^{'}} - k_{rj}\prod_{i=1}^{N}\left[X_i\right]^{v_{ij}^{*}} \tag{15}$$

The reaction rate of the global chemical reaction in Eqs. (10) and (11) are given by

$$q_1 = A_1\left[CH_4\right]^{n1}\left[O_2\right]^{n2}\exp\left(-\frac{Ea_1}{Ru\cdot T}\right) \tag{16}$$

$$q_2 = A_2\left[\left[CO\right]^{m1}\left[O_2\right]^{m2} - \frac{1}{K_{eq}}\left[CO_2\right]^{m3}\right]\mathrm{T}^{0.7}\exp\left(-\frac{Ea_2}{Ru\cdot T}\right) \tag{17}$$

Dryer F L and Westbrook C K propose that the concentration of exponents in each reaction cannot be defined from the stoichiometric coefficient, otherwise flame destabilizes inside the reactor [8]. The requisite parameter to calculate reaction are in Eqs (15) and (16) are provided in Table 1. The unit of the pre-exponential constant is in cgs and activation energy is in [J/kmol].

Table 1: The constant parameter for the reduced mechanism [11].

No.	Pre-exponential factor	Activation Energy	Rate Exponents
Reaction 1	$A_1=1.7386\times10^9$	$Ea_1=1.48532\times10^8$	$n_1=0.5$, $n_2=0.65$
Reaction 2	$A_2=6.325\times10^6$	$Ea_2=5.0208\times10^7$	$m_1=m_3=1$, $m_2=0.5$

2.1.2 Boundary conditions

At the inlet of the free flow domain

$T_g = T_s = T = 300K, \quad u_z = u_0 \quad \text{and} \quad u_r = 0$

$Y_{CH_4} = Y_{CH_4,in} \quad \text{and} \quad Y_{O_2} = Y_{O_2,in}$

At the outlet of the computational domain

$\frac{\partial \mathrm{T}}{\partial \mathrm{z}} = \frac{\partial \mathrm{Y_i}}{\partial \mathrm{z}} = \frac{\partial \mathrm{u_z}}{\partial \mathrm{z}} = 0 \quad \text{and} \quad \mathrm{P_{out}} = 0 \text{ atm}$

No-slip boundary condition is applied to the wall of both free flow and porous media flow domain. The condition prescribes u equal to zero; it means that the fluid at the wall is not moving. Plus, the radiation and convection heat loss is accounted for by the following expression

$$\lambda_w \frac{\partial T_w}{\partial z} = h_{air}\left(T_{ex} - T_{amb}\right) + \varepsilon_w \sigma\left(T_{ex}^4 - T_{amb}^4\right)$$

The convection heat transfer coefficient h_{air} is approximately equaled to 2 W/(m^2·K) which accounts for heat loss by conduction through isolator and natural convection of insulator wall and ambient air. surface emissivity for radiation is set to 0.3 and the ambient temperature for each case is 303.15 K.

3. RESULTS AND DISCUSSION

3.1. Species concentration and temperature contours in the reaction engineering module

Under the condition of Batch constant volume with the initial temperature of 300 K. Fig. 2a illustrate that temperature is increased up to more 3600 K and the reaction happens very fast as shown in Fig. 2b. However, this kind of result does not make a significant impact on the analysis. It only uses to provide thermodynamic and transport data to the chemical and other interfaces to analyze porous media combustion.

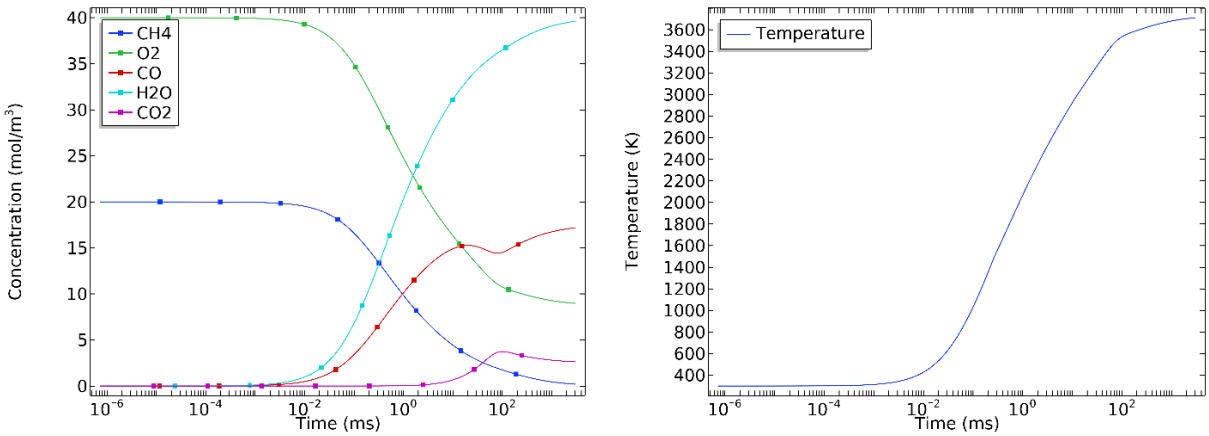

(a) (b)

Fig. 2. Species concentration (a) and temperature profile (b)

3.2 Temperature

The second step of the multiphysics coupling interprets that the peak temperature of this burner approximately reaches up to 560 °C as shown in Fig. 3. Fig. 3a shows the temperature inside the combustion chamber (porous media domain). And Fig. 3b shows the temperature profile in the axial direction. The temperature increases dramatically from 30 °C at 0.047 m in z-coordinate to 569 °C at z equal to 0.06 m. Then, heat is distributed across the fluid and porous media domain. The temperature is gone down a little bit due to heat loss through the combustion chamber wall. Finally, the temperature has remained only 495 °C at the end of the burner.

3.3 Pressure and velocity

In general, the pressure is increased at the inlet due to porous media flow resistance. The reference value of pressure is set to be one atmosphere. In porous media, permeability expresses as the ability of the porous medium to carry fluid from one point to another. The pressure field has a significant effect on this parameter. For instance, the pressure is increased if the permeability increases. In fact, the pressure deviation of this study is slightly different. Thus, it was assumed to be constant. The fully developed average velocity enters at the inlet boundary condition. The velocity almost equally in magnitude when it enters the porous domain as shown in Fig. 4a. Noticeably, there is a big void at the side end of the inlet pipe where the domain is transited beside the majority of the flow is distributed to the wall. This will cause some problems when the burner size is increasing as represent in Fig. 4b. More precisely, the flame is burned near the chamber wall instead of the middle.

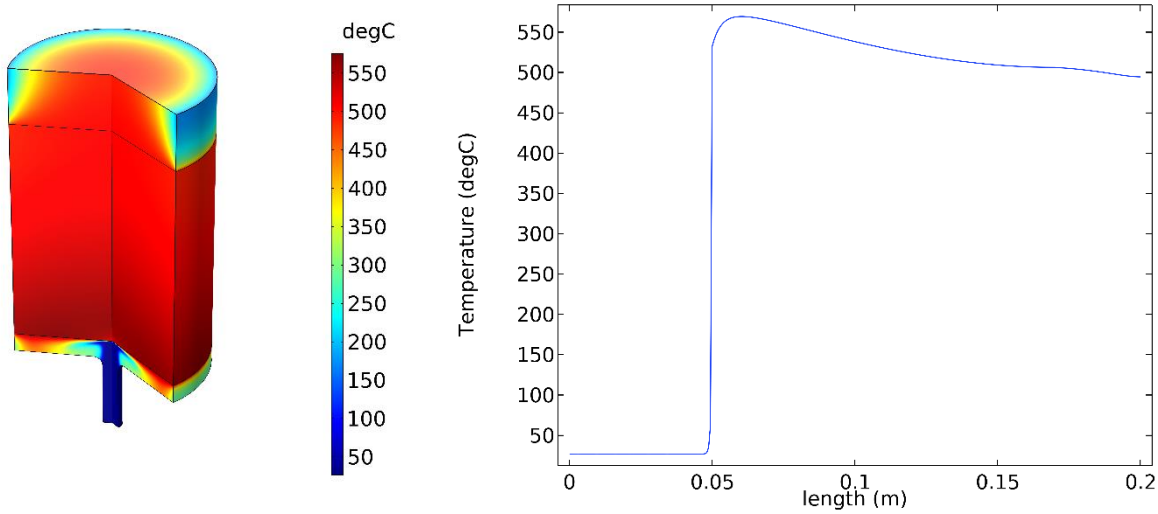

(a) (b)

Fig. 3. Temperature profile in (a) 3D axisymmetric and (b) axial direction.

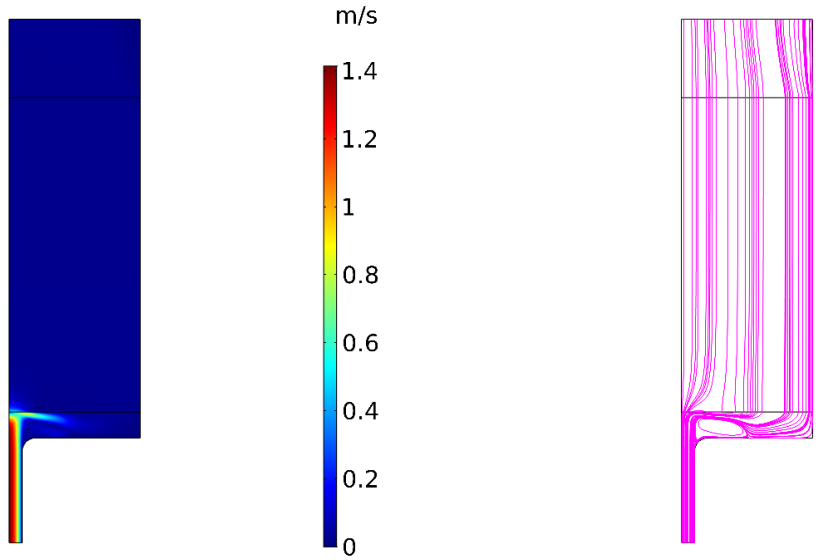

(a) (b)

Fig. 4. Velocity field (a) and streamline (b).

3.4 Molar concentration of each species

As display in Fig. 5a shows the concentration of methane and Fig. 5b shows the concentration of oxygen, there is no amount of fuel left after the combustion occurs. However, a little bit amount of oxygen remaining. The concentration of each species rapidly changes at the bottom of the combustion chamber.

At domain (1) which is the fluid domain, the molar concentration of both carbon monoxide (Fig. 6a) and water (Fig. 6b) does not exist until the combustion occurs at the porous domain. The product of the chemical reaction produces a small amount of these species. From a pollutant perspective, less generation of carbon monoxide and dioxide after combustion is always the key focus in the combustion community.

It is clearly seen that the formation of carbon dioxide is pretty small compare with the other species. Starting from the inlet boundary condition to the middle of the porous domain the presence of the molar concentration of carbon dioxide is almost zero. It immediately generates a bit afterward. The maximum concentration of this species occurs at the very end of the combustion chamber close to the wall as illustrated in Fig. 7.

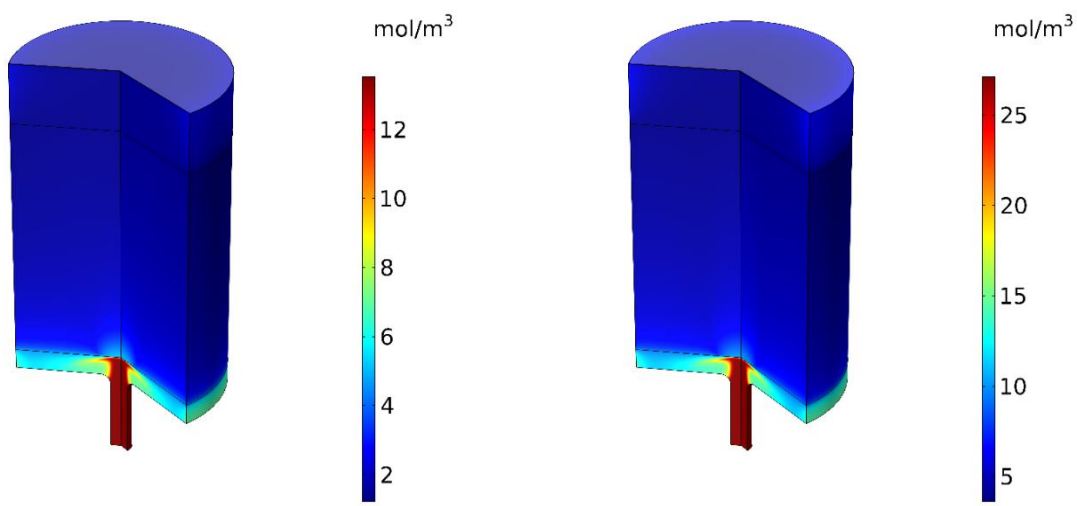

(a) (b)

Fig. 5. Species concentration of methane (a) and oxygen (b).

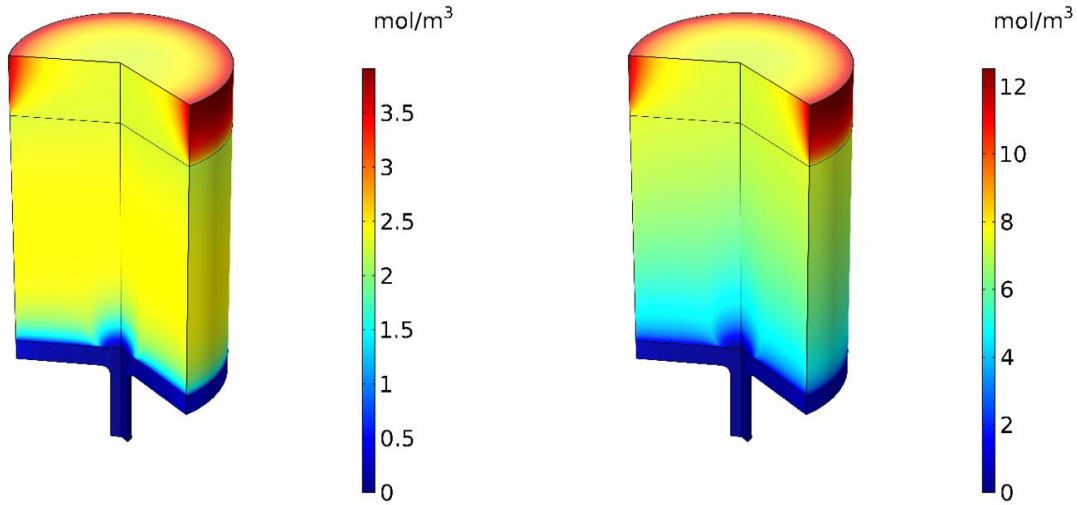

(a) (b)

Fig. 6. Molar concentration of carbon monoxide (a) and water (b).

4. CONCLUSION

The flow, heat transfer, and combustion in porous media have been examined. The combustion reaction is modeled by a reduced reaction mechanism and energy equations are solved under the assumption of local thermal equilibrium. The temperature and chemical species formation in the porous media is presented in a streamlined and three-dimensional space. It is observed that the highest temperature has occurred at the end of the porous domain and the beginning of the fluid outlet domain. It can only occur in the porous media burner due to the advantages of high thermal radiation of porous material. What is more, the numerical simulation result can provide data such as temperature, pressure, and species concentration at any point inside the system. This information is handy to optimize the most efficient porous media combustor.

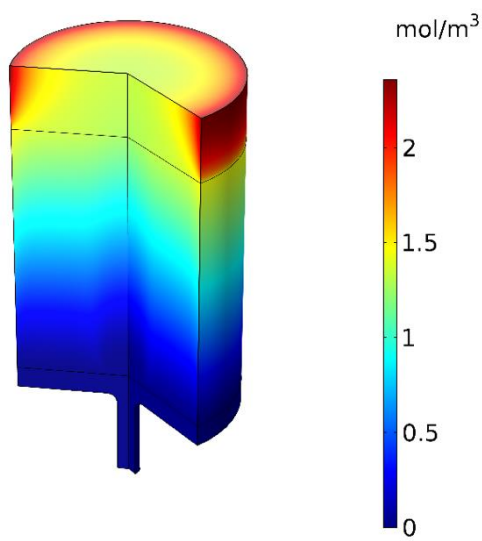

Fig. 7. Molar concentration of carbon dioxide.

ACKNOWLEDGMENTS

This work was supported by National Energy Technology Center (ENTEC). The author would like to acknowledge TAIST Tokyo Tech for their financial support during the period of the study.

NOMENCLATURE

ρ	density of premixed gas, kg/m^3
ε_p	porosity of the porous medium
$\boldsymbol{u}$	averaged velocity vector of the mixture, m/s
μ	dynamic viscosity of the fluid, Pa·s
β	inertial resistance coefficient, m^{-1}
c_F	Forchheimer parameter
P	pressure, Pa
T	temperature, K
d_p	spherical porous media diameter, m
C_p	fluid heat capacity at constant pressure, J/(kg K)
k_{eff}	effective thermal conductivity, W/(m K)
Q	heat source or sink, W
Q_{vd}	viscous dissipation in the fluid,
$\boldsymbol{j}_i$	mass flux relative to the mass averaged velocity, kg/(m^2·s)
Y_i	mass fraction of
q_j	rate expression of its production or consumption, kg/ (m^3·s)
$\dot{\omega}_i$	net production rate of ith species
D_i^m	mixture-averaged diffusion coefficient
D_i^T	thermal diffusion coefficient, kg/(m·s)
M_n	mean of molar mass, kg/mol
M_i	molar mass of ith species, kg/mol
Ru	universal gas constant, 8.314 J/(mol· K)
X_i	mole fraction of ith species
$v_{ij}^{'}$	stoichiometric coefficients on the reactants for jth reaction and ith species
$v_{ij}^{''}$	stoichiometric coefficients on the product for jth reaction and ith species
k_{fj}	forward rate coefficient of jth reaction
k_{rj}	reverse rate coefficient of jth reaction
k_{eq}	equilibrium constant
A	pre-exponential factor
Ea	activation energy
h_{air}	convection heat transfer coefficient, 2 W/(m^2·K)
ε_w	surface emissivity for radiation, 0.3

Subscripts

i	ith species
j	jth reaction
g	gas
s	solid
w	wall
in	inlet

out	outlet
ex	exterior
amb	ambient
f	forward
r	reverse

REFERENCES

[1] Takeno, T., Sato, K., Hase, K. A theoretical study on an excess enthalpy flame, Symposium (International) on Combustion, Vol. 18, 1981, pp. 465-472.

[2] Weinberg, F.J. Combustion temperatures: the future?, Nature, Vol. 233, 1971, pp. 239-241.

[3] Drayton, M.K, Saveliev, A.V., Kennedy, L.A., Fridman, A.A., Li, Y.E. Syngas production using superadiabatic combustion of ultra-rich methane-air mixtures, Symposium (International) on Combustion, Vol. 27, 1998, pp. 1361-1367.

[4] Zhang, L., Xu, R., Jiang, P. Comparison of volume-averaged simulation and pore-scale simulation of thermal radiation and natural convection in high temperature packed beds, paper presented in 5th International Conference on Porous Media and Their Applications in Science, Engineering and Industry, 2014, Kona, Hawaii.

[5] Sobhani, S., Haley, B., Bartz, D., Dunnmon, J., Sullivan, J., Ihme, M. Investigation of lean combustion stability, pressure drop, and material durability in porous media burners, paper presented in ASME Turbo Expo: Power for Land, Sea, and Air, 2017, North Carolina, USA.

[6] Shi, J.R., Yu, C.M., Li, B.W., Xia, Y.F. Xue, Z. Experimental and numerical studies on the flame instabilities in porous media, Fuel, Vol. 106, 2013, pp. 674-681.

[7] Zeng, K.L. Application & Manufacture of Porous Media Ceramics, 2006, Beijing Chemical Industry Press, China.

[8] Franzelli, B., Riber, E., Sanjosé, M., Poinsot, T. A two-step chemical scheme for kerosene-air premixed flames, Combustion and Flame, Vol. 157(7), 2010, pp. 1364-1373.

[9] Dryer, F.L. and Westbrook, C.K. Simplified reaction mechanisms for the oxidation of hydrocarbon fuels in flames, Combustion Science and Technology, Vol. 27, 1981, pp. 31-43.

[10] Franzelli, B., Riber,E., Gicquel, L.Y.M., Poinsot, T. Large Eddy Simulation of combustion instabilities in a lean partially premixed swirled flame, Combustion and Flame, Vol. 159(2), 2012, pp. 621-637.

[11] Deng, H., Huang, M., Wen, X., Chen, G., Wang, F., Yao, Z. Numerical investigation of premixed methane-air flame in two-dimensional half open tube in the early stages, Fuel, Vol. 272, 2020, pp. 117709.